

Numerical Heat Transfer, Part A: Applications



An International Journal of Computation and Methodology

ISSN: (Print) (Online) Journal homepage: www.tandfonline.com/journals/unht20

Numerical analysis of transient MHD natural convection in a channel with four heat-generating cylindrical solids filled with in a non-Newtonian Fe₃O₄ ferrofluid

Massinissa Adnani, Adel Sahi, Bachir Meziani, Abdelhakim Benslimane & Ali J. Chamkha

To cite this article: Massinissa Adnani, Adel Sahi, Bachir Meziani, Abdelhakim Benslimane & Ali J. Chamkha (07 Aug 2024): Numerical analysis of transient MHD natural convection in a channel with four heat-generating cylindrical solids filled with in a non-Newtonian Fe_3O_4 ferrofluid, Numerical Heat Transfer, Part A: Applications, DOI: 10.1080/10407782.2024.2388239

To link to this article: https://doi.org/10.1080/10407782.2024.2388239

	Published online: 07 Aug 2024.
Ø.	Submit your article to this journal 🗹
ď	View related articles 🗹
CrossMark	View Crossmark data 🗗





Numerical analysis of transient MHD natural convection in a channel with four heat-generating cylindrical solids filled with in a non-Newtonian Fe₃O₄ ferrofluid

Massinissa Adnani^a (D), Adel Sahi^b (D), Bachir Meziani^c (D), Abdelhakim Benslimane^b (D), and Ali J. Chamkha^d (D)

^aFaculté de Technologie, Laboratoire de Physique Théorique, Université de Bejaia, Algeria; ^bFaculté de Technologie, Laboratoire de Mécanique, Matériaux et Energétique (L2ME), Université de Bejaia, Algeria; ^cFaculté des Sciences Exactes, Laboratoire de Physique Théorique, Université de Bejaia, Algeria; ^dFaculty of Engineering, Kuwait College of Science and Technology, Doha, Kuwait

ABSTRACT

This article presents a numerical investigation and analysis of the cooling effectiveness of thermomagnetic transient natural convection in a long channel, equipped with four cylindrical heat-generating blocks. A non-Newtonian power-law ferrofluid was employed for the present investigation to achieve optimum cooling. The governing equations are the continuity equation, the momentum equation and the energy equation. The finite volume method was used to solve the resulting algebraic system. From an energy-saving point of view, this configuration can provide a good approximation for selecting effective physical and geometrical parameters to design a reliable thermal system. For this purpose, the study was carried out for various geometric and thermophysical parameters. Different values of thermal conductivity, power law index, Rayleigh number, Hartmann number and ferrofluid volume fraction, were considered. The results are illustrated in the form of streamlines, isotherms, average Nusselt and a spatio-temporal characterization of the mean ferrofluid velocity. From the results presented, we can conclude that the choice of non-Newtonian, pseudoplastic ferrofluid with a low thermal conductivity ratio subjected to a uniform magnetic field proves to be a crucial solution for efficient and stable cooling of heat-generating cylindrical blocks, which will have to be close to the cold walls of the channel.

ARTICLE HISTORY

Received 6 May 2024 Revised 28 July 2024 Accepted 30 July 2024

KEYWORDS

Ferrofluid; hartmann; long channel; natural convection; non-Newtonian

1. Introduction

In the field of heat transfer, nano-additives stand out for their high thermal conductivity and enhanced system stability compared with base fluids. For example, incorporating nanoparticles into the base fluid can help improve the thermal convection cooling of a system with a typical internal energy source. Researchers are constantly striving to discover new ways of increasing the efficiency of energy devices [1, 2].

In order to minimize the risk of equipment damage or malfunction, the analysis of natural convection in enclosures containing heat-generating solids is recognized as a promising solution. The preference for natural convection is explained by its widespread use in technical applications, positioning it advantageously over other convective processes, such as cooling operations in

Nomenclature					
A*	dimensionless cylinder surface	U, V	non-dimensional horizontal and vertical		
В	strength of magnetic influence (kg/		velocities		
	s ² /amp)	x, y,z	dimensional Cartesian coordinates (m)		
Ср	specific heat (J kg ⁻¹ k ⁻¹)	X, Y, Z	non-dimensional Cartesian coordinates		
D	strain rate tensor				
g	gravitational acceleration (m s ⁻²)	Greek sym	ibols		
Ha	Hartmann number	α	heat diffusivity (m ² s ⁻¹)		
Н	channel height (m)	β	heat expansion coefficient (K ⁻¹)		
k	thermal conductivity (W m ⁻¹ K ⁻¹)	ν	kinematic viscosity (m ² s ⁻¹)		
k*	thermal conductivity ratio	μ	dynamic viscosity (kg m ⁻¹ s ⁻¹)		
L	dimensional size of the channel (m)	φ	nano-sized particles volume fraction		
m	consistency	ρ	density (kg m ⁻³)		
n	power-law index	, (ρCp)	heat capacitance (J K ⁻¹ m ⁻³)		
N	aspect ratio of the channel	$(\rho\beta)$	thermal expansion (10^{-6}K^{-1})		
Nr	aspect ratio of the solid body	σ	electrical conductivity (Ωm) 1		
Nx, Ny	Dimensionless of the position of the solide	$ heta \! f \! f$	non-dimensional temperature for a fluid		
	body	55	region		
Nu	local Nusselt number	θs	non-dimensional temperature for a solid		
p	dimensional pressure (N m ⁻²)		region		
P	dimensionless pressure	τ	non-dimensional time		
Pr	Prandtl number	Υ	strain rate tensor (N m ⁻²)		
q"	Uniform heat generation rate (Wm^{-3})				
Ra	Rayleigh number	Subscripts			
r	dimensional radius of the solid body (m)	Avg	average		
t	dimensional time (s)	C	cold		
$T_{\rm ff}$	dimensional temperature for a fluid	f	fluid		
	region,(K)	ff	ferrofluid		
T _s	dimensional temperature for a solid region	max	maximum		
	(K)	p	particle		
T _c	dimensional cold wall temperature (K)	S	solide		
u,v	dimensional horizontal and vertical veloc-	sf	surface		
	ities (m s ⁻¹)	i,j	tensor index		

electronic equipment, nuclear and chemical reactors and heat exchangers. Heat transfer by natural convection can be enhanced by modifying the shape of the geometry with variable boundary conditions [3, 4], or with the addition of nanoparticles to the base fluid [5].

Researchers have developed tools and techniques to control and improve the rate of heat transfer during natural convection, D. Mansoury *et al.* [6] and L. Snoussi *et al.* [7].

Mokaddes et al. [8] presented a study of natural convection induced by the insertion of a cylindrical heat-generating block into a cavity with a corrugated wall. In the course of their investigations, it was found that the force of fluid movement is more pronounced in a corrugated cavity containing a heat-generating obstacle than in a smooth cavity with no obstacle. A numerical study of natural convection around two cylinders maintained at a temperature difference with the same geometric shape was carried out by M. Boukendil et al. [9]. The results show that location, cylinder shape and Rayleigh number play an important role in convective heat transfer. With the aim of maintaining ambient temperature uniformity and avoiding excessive cooling of an electronic device, M. Foruzan et al. [10] have numerically examined the heat dissipation generated in the latter. The results show that a higher cooling rate can be achieved during the transient period for a higher surface emissivity and a higher Plank number. The effect of the uniform Lorentz force on energy transport and cooling by thermomagnetic convection was examined by C. Sivaraj et al. [11] and S. Priyadharsini et al. [12] respectively in a cavity containing a heat-generating

solid. The results indicate that an increase in the magnetic parameter Ha leads to a reduction in heat transfer. And, the addition of nanometer-sized particles improves energy transport. Furthermore, an improvement in cooling was indicated by decreasing the aspect ratio of the heat-generating solid block.

Ferrofluid, also known as magnetic colloid, is a suspension of nano-sized Fe oxide (Fe₃O₄) particles in a base fluid with low thermal conductivity. Oil, water and ethylene-glycol mixtures are generally considered as base fluids. Ferrofluids can be used to enhance heat transfer in a thermal system [13, 14]. By adjusting the magnetic properties of the fluid, it is possible to control its viscosity and thus its ability to transport heat. This optimizes heat transfer in targeted areas of the system, improving its overall efficiency.

Ferrofluids have made considerable progress in recent decades. This is mainly due to the widespread use of nanotechnologies in industrial and engineering products. The temperature rise of an electrically heated wire immersed in a ferrofluid has been studied analytically and experimentally by A. Vatani et al. [15] in the case of thermomagnetic convection. The hydrothermal characteristics of the Fe₃O₄ ferrofluid are studied by M. Bahiraei et al. [16]. The placement of four magnets was suggested by the authors to improve heat transfer. Natural convection heat transfer performance of aqueous Fe₂O₃-Al₂O₃ nanofluids under the influence of magnetic induction was studied and discussed by S. O. Giwa et al. [17]. During this research, the authors show that heat transfer performance depended on the choice of nanoparticles. Furthermore, the boundary layer flow around a rotating vertical cone placed in a hybrid ferrofluid was studied by S. Saranya et al. [18]. The results show that a hybrid ferrofluid produces maximum skin friction and maximum heat transfer compared with base fluids and simple nanofluids. Y. Cao et al. [19] conducted a study of natural convection in a cavity filled with Fe₃O₄ ferrofluid. They showed that the Nusselt number is increased by 32% for a volume fraction of 0.01 to 0.03. An experimental study of the hydrothermal behavior of Fe₃O₄ ferrofluid flowing under the effect of a uniform magnetic field was carried out and discussed by E. Gürsoy et al. [20]. The authors shed light on the study of ferrofluid behavior under the influence of a variable magnetic field. The influence of a nonuniform magnetic field on heat transfer and entropy production in a cavity filled with a ferrofluid was studied by B. Iftikhar et al. [21]. The results show that fluid velocity and entropy production decrease with increasing magnetic number. M. Nemati et al. [22] analyzed the cooling of a hot body by natural convection in an inclined trapezoidal geometry. They showed that the optimum thermal performance coefficient of the system can be achieved with the maximum Rayleigh value and the minimum Hartmann value, in the absence of heat absorption for the shear-thinning fluid. K. Gangadhar et al. [23] examined and evaluated a micropolar ferrofluid's flow and heat transfer properties. The findings indicate that compared to a traditional micropolar fluid, the micropolar ferrofluid has a larger energy distribution. The objective of the investigation of [24] is to examine how the shape of the nanoparticles affects the magnetohydrodynamic free convection heat transfer performance and thermo-physical parameters of the water-based magnesium ferrite ferrofluid. It was found that the thermo-physical properties of ferrofluid were enhanced by the inclusion of cube-shaped magnesium ferrite particles.

The use of non-Newtonian fluids in a cooling system can offer advantages such as increased viscosity control, reduced pressure drop, resistance to flow variations and better management of mechanical stress, all of which can contribute to improving overall system efficiency and reliability. Non-Newtonian fluids are characterized by their non-linear viscosity, and are frequently encountered in industrial applications. Solvents, molten polymers, viscoelastic materials and atomic fluids are all examples of fluids with non-Newtonian properties. Understanding the transmission indicators of these fluids is of particular importance for these specific applications. In recent years, several scientific studies have focused on the circulation of fluids, whether Newtonian or non-Newtonian, within a closed cavity. The effect of a non-Newtonian shearthinning viscosity has been studied by K. Khellaf et al. [25], H. Demir et al. [26] and Z. Alloui

et al. [27]. Their results reveal the strong influence of the pseudoplastic behavior of a fluid governed by an index power law (n < 1) on its heat transfer by natural convection. Furthermore, A. Boutra et al. [28] reported that an increase in maximum temperature was found using a dilatant fluid (n > 1) in the presence of a heat-generating obstacle instead of pseudoplastic and Newtonian fluids (n < 1, n = 1). R. R. Kairi et al. [29] Analyzed the influence of viscous dissipation from a vertical cone in a non-Darcy porous medium saturated with a non-Newtonian fluid. The results show that heat transfer decreases as the dissipation parameter increases for all fluid types (n < 1,n=1 and n>1). On the other hand, due to viscous resistance, S. Yigit et al. [30] have shown that a weakening of thermal advection was reported when the power law index becomes large (n > 1). The non-Newtonian behavior of a phase change material (PCM) was studied by M. Ghalambaz et al. [31]. The results show that a decrease in the power law index can significantly increase the melting rate. Furthermore, correlations linking Nu to the power law index n as a function of control parameters have been proposed by L. Khezzar et al. [32] in the case of natural convection in cavities filled with non-Newtonian power law fluids. Hussan Zeb et al. [33] Analyzed the heat transfer characteristics of non-Newtonian ferrofluids produced by a stretch film. The authors show that the concentration, temperature and velocity field are influenced by control parameters. The uniform transpiration rate on boundary layer flow by natural convection of a non-Newtonian fluid was studied and analyzed by A. M. Rashad et al. [34], the results revealing that increasing viscosity index values lead to increased heat transfer. P. P. Roy et al. [35] examined the thermal performance of a power law fluid for an enclosure heated discretely by a cover. The authors show that heat transfer is inversely proportional, in the case of forced and natural convection, as a function of the power law index. All these conclusions were verified experimentally by Agool et al. [36] in the case of a rectangular cavity containing a hot obstacle. In addition, the authors demonstrated that the cylindrical shape of the obstacle improves heat transfer more than the cubic shape. The natural laminar convection of a long heated cylinder immersed in a non-Newtonian power-law fluid was studied numerically by C. Sasmal et al. [37], and the authors were able to show the consistency of their results with the experimental data available in the literature. The three-dimensional case of a non-Newtonian fluid in a thick-walled container was studied and analyzed by N. O. Moraga et al. [38]. The results show that a narrow thermal plume in air in the case of a Newtonian fluid differs from the non-Newtonian one around the inner cavity. The flow of a viscoelastic Casson fluid in a square cavity in the presence of an external magnetic field is examined numerically by T. Sarala Devi et al. [39] The results indicate that the temperature gradient is an increasing function of the buoyancy force. D. S. Loenko et al. [40] The time dependence of a sinusoidal temperature profile on the natural convection of a non-Newtonian fluid was analyzed. The results show that, at high oscillation frequencies of a pseudoplastic fluid (n < 1), convective transfer intensifies at very high Rayleigh. J.-F. Xie et al. [41] studied the natural convection of non-Newtonian power-law fluids in the presence of wall vibrations in a rectangular cavity. It has been observed that when aspect ratio and Pr increase, the rate of heat transret decreases. S. Doley et al. [42] focused on heat transfer between the ambient medium and the moving material under MHD radiative-convection, viscous dissipation effects, and time-fractional condition. To examine fluid flow along a vertical plate with impulsive startup, the authors established a mathematical model that describes a hybrid nanofluid by considering the transient term as a fractional derivative. Their results show that changing the fractional order affects flow and heat transfer. A. Divya et al. [43] Numerically analyzed naturally convective MHD flow through an exponentially accelerating plate with viscous dissipation. The main results show that primary velocity, transverse velocity, temperature and concentration profiles are affected by variations in system control parameters.

During the literature survey, we were able to show that non-Newtonian power law fluids can play an important role in improving convective transfer. Therefore, for efficient cooling, it is important to add nano-sized Fe oxide additives to the base fluid. That is why we chose a non-

Newtonian power-law Ferrofluid Fe₃O₄ to study the efficiency of heat transfer by transient natural convection. The use of non-Newtonian ferrofluid in a thermal system containing cylindrical heat-generating blocks offers the possibility of precisely controlling heat transfer, ensuring uniform heat distribution, managing mechanical constraints, designing systems that are more compact and benefiting from rapid response to changing conditions. In addition, to control and reduce heat transfer and avoid the risk of system damage or malfunction, a magnetic field was imposed in the positive direction along the x-axis. This question is crucial to improving the design and performance of thermal and energy systems. This research can lead to significant advances in the understanding of complex heat and fluid transfer phenomena, as well as in the development of more efficient and innovative technologies.

To this end, the main objective of this study is to analyze the effect of the magnetic field, temperature gradient, aspect ratio and position of the heat-generating blocks on transient natural convection. Variations in the thermal conductivity of the heat-generating blocks, power law index n and nanoparticle volume fraction are also taken into account. The novelty of this work lies in the fact that the two-dimensional temperature distribution of the solid phase in cylindrical coordinates and the fluid phase in Cartesian coordinates is obtained separately, with special dimensionless modeling brought in on the magnetic field strength, notably the Hartmann number. The results of this study are directly applicable to the cooling of high-power electronic components. By optimizing cooling systems through a better understanding of thermal and fluidic interactions, this research can contribute to significant advances in the thermal management of modern electronic devices.

The results will be illustrated in the form of streamlines, isotherms, average Nusselt number and a spatio-temporal characterization of the mean ferrofluid velocity.

2. Physical and mathematical formulation

This study presents an analysis of transient natural convection cooling of a channel with aspect ratio N = H/L. The channel is long enough for the system to reduce to 2D and is equipped with four cylindrical heat-generating blocks, each with a different aspect ratio and distinct position $(N_x = \delta x_i/L, N_y = \delta y_i/L, N_r = r/L)$, Figure 1. The left, right and bottom walls of the channel are considered adiabatic, while cooling by a cold temperature T_C is applied to the top wall. The internal cylinders are assumed to generate heat at a uniform rate qo. Heat transfer and flow induced by a vertical temperature gradient are assumed to be laminar and two-dimensional in the transient regime. The Fe oxide (Fe₃O₄) and the base fluid are in thermal equilibrium, and their properties are assumed to be constant, Table 1. The ferrofluid is non-Newtonian power-law, incompressible and the Boussinesq approximation is applied. To control the heat transfer mechanism, a uniform magnetic field of force B is imposed on the positive direction following the xaxis. Radiation effects are neglected.

Considering the above assumptions, the equations governing the conservation of mass, momentum and energy can be transcribed in the following dimensional form;

$$\frac{\partial u}{\partial x} + \frac{\partial v}{\partial x} = 0 \tag{1}$$

$$\rho_{ff}\left(\frac{\partial u}{\partial t} + u\frac{\partial u}{\partial x} + v\frac{\partial u}{\partial y}\right) = -\frac{\partial p}{\partial x} + \left(\frac{\partial \Upsilon_{xx}}{\partial x} + \frac{\partial \Upsilon_{xy}}{\partial y}\right)$$
(2)

$$\rho_{ff}\left(\frac{\partial v}{\partial t} + u\frac{\partial v}{\partial x} + v\frac{\partial v}{\partial y}\right) = -\frac{\partial p}{\partial y} + \left(\frac{\partial \Upsilon_{xy}}{\partial x} + \frac{\partial \Upsilon_{yy}}{\partial y}\right) + (\rho\beta)_{ff}g(T - T_c) - \sigma_{ff}B_0^2v \tag{3}$$

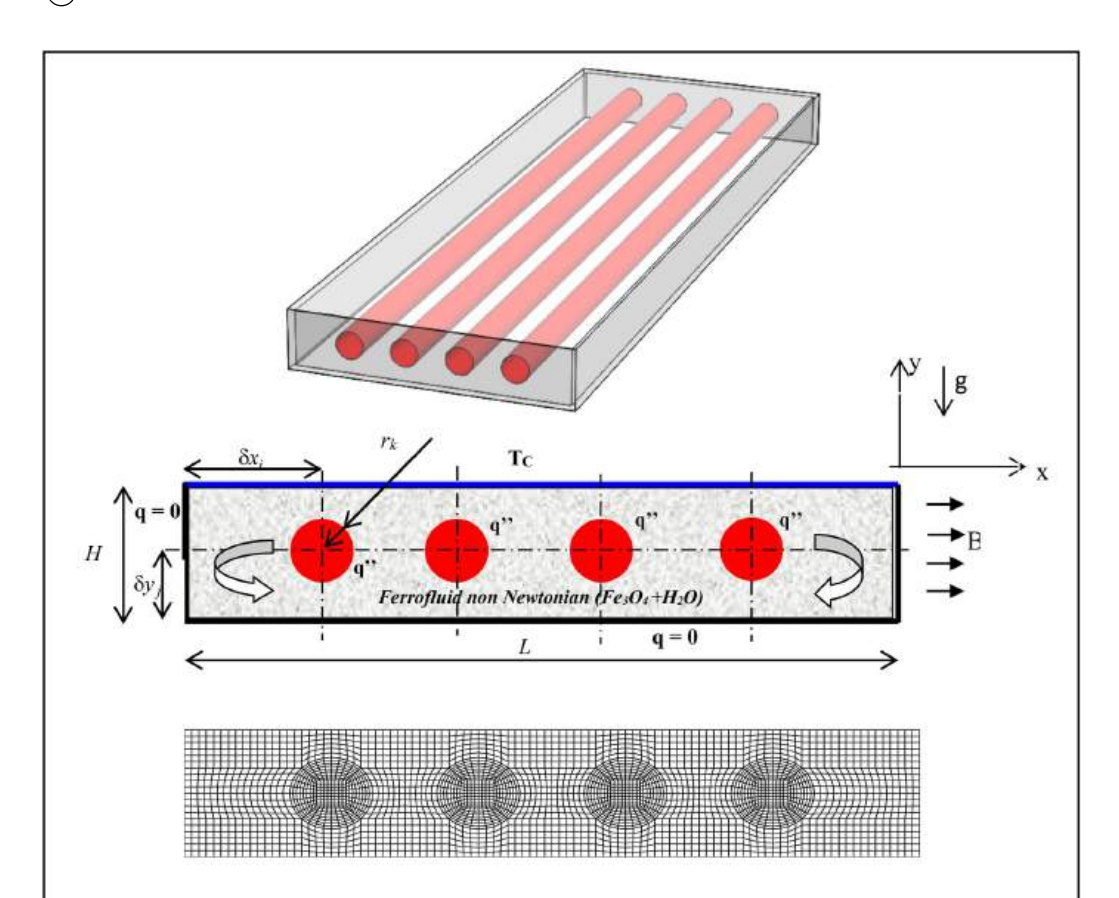


Figure 1. Physical formulation.

Table 1. Average nusselt number compared with data of.

Physical properties	Base fluid	Ferro nanoparticles Fe ₃ O ₄
$Cp [J kg^{-1} K^{-1}]$ $\rho [kg m^{-3}]$	4179	670
ρ [kg m ⁻³]	997.1	5200
$k \text{ [W m}^{-1} \text{ s}^{-1}]$	0.613	6
σ [S m ⁻¹]	0.05	25000
$\beta \times 10^{-5} [K^{-1}]$	20.7	1.18
$\beta \times 10^{-5} [K^{-1}]$ $\mu [kg m^{-1} s^{-1}]$	0.001003	_

$$\frac{\partial T_{ff}}{\partial t} + u \frac{\partial T_{ff}}{\partial x} + v \frac{\partial T_{ff}}{\partial y} = \left(\frac{k}{\rho C_P}\right)_{ff} \left(\frac{\partial^2 T_{ff}}{\partial x^2} + \frac{\partial^2 T_{ff}}{\partial y^2}\right), \text{ for the ferrofluid zone}$$
(4)

$$\frac{\partial T_s}{\partial t} = \left(\frac{k}{\rho C_P}\right)_s \left(\frac{\partial^2 T_s}{\partial r^2} + \frac{1}{r} \frac{\partial T_s}{\partial r} + \frac{\partial^2 T_s}{\partial z^2}\right) + q_{gen}^{"}, \text{ for the solid zone heat source}$$
 (5)

For a non-Newtonian power law fluid, the viscous stress tensor is given by [44].

$$\Upsilon_{ij} = 2\mu_a D_{ij} = \mu_a \left(\frac{\partial u_i}{\partial x_i} + \frac{\partial u_j}{\partial x_i} \right)$$
 (6)

Where Dij is the strain rate tensor for the two-dimensional Cartesian coordinate. The apparent viscosity in is given by Eq. (7) below.



$$\mu_{a} = m \left\{ 2 \left[\left(\frac{\partial u}{\partial x} \right)^{2} + \left(\frac{\partial v}{\partial y} \right)^{2} \right] + \left(\frac{\partial v}{\partial x} + \frac{\partial u}{\partial y} \right)^{2} \right\}^{\frac{n-1}{2}}$$
 (7)

Where m and n are power-law model constants, m is the consistency coefficient and n is the power-law index. Under shear, when (n < 1), the fluid is pseudoplastic, (n > 1), the fluid is dilatant and when (n = 1), the fluid is Newtonian.

The following boundary conditions are taken into account in this study:

- $t = 0 : u = v = 0, T_{ff} = T_{avg}, 0 \le x \le L \text{ and } 0 \le y \le H$

$$u = v = 0, \quad T_{ff} = T_c, \quad 0 \le x \le L, \quad y = h$$

$$u = v = 0, \quad \frac{\partial T_{ff}}{\partial y} = 0, \quad 0 \le y \le h, \quad x = 0, \quad x = L \quad and \quad 0 \le x \le L, \quad y = 0$$

$$u = v = 0, \quad k_k \frac{\partial T_f}{\partial n} = k_s \frac{\partial T_s}{\partial n}, \quad \text{at the fluid - solid interface}$$
(8)

The effective density, specific heat and coefficient of thermal expansion of ferrofluid can be expressed as follows [1, 45]:

$$\rho_{ff} = (1 - \varphi)\rho_f + \varphi\rho_p, \ (\rho C_P)_{ff} = (1 - \varphi)(\rho C_P)_f + \varphi(\rho C_P)_p, \ (\rho \beta)_{ff} = (1 - \varphi)(\rho \beta)_f + \varphi(\rho \beta)_p$$
(9)

The effective thermal conductivity of the ferrofluid is defined using the Maxwell Garnett method [42, 46].

$$k_{ff} = k_f \left[\frac{k_p + 2k_f - 2\varphi(k_f - k_p)}{k_p + 2k_f + 2\varphi(k_f - k_p)} \right]$$
(10)

The standard effective viscosity given by Brinkmann [47] is

$$\mu_{ff} = \frac{\mu_f}{(1 - \omega)^{2.5}} \tag{11}$$

The effective electrical conductivity of the ferrofluid can be given by the following Eq. (12) [48, 49].

$$\sigma_{ff} = \sigma_f \left[\frac{\sigma_p + 2\sigma_f - 2\varphi(\sigma_f - \sigma_p)}{\sigma_p + 2\sigma_f + 2\varphi(\sigma_f - \sigma_p)} \right]$$
(12)

With the introduction of the following dimensionless parameters;

$$X = \frac{x}{L}, \quad Y = \frac{y}{L}, \quad R = \frac{r}{L}, \quad Z = \frac{z}{L}, \quad U = \frac{uL}{\alpha_f}, \quad V = \frac{vL}{\alpha_f}, \quad P = \frac{pL^2}{\rho\alpha_f^2},$$

$$\tau = \frac{t\alpha_f}{L^2}, \quad \theta_{ff} = \frac{T_{ff} - T_c}{\Delta T}, \quad \theta_s = \frac{T_s - T_c}{\Delta T}, \quad \Delta T = \frac{q''_{gen}\pi r^2}{k_f}, \quad Ra = \frac{g\beta_f \Delta T L^{2n+1}\rho_f}{\alpha_f^n m},$$

$$Pr = \frac{mL^{2n-2}}{\rho\alpha_f^{2-n}}, \quad Ha = L^n B_0 \sqrt{\frac{\sigma_f}{m\alpha_f^{n-1}}}, \quad A^* = \frac{\pi r^2}{L^2}, \quad \alpha^* = \frac{\alpha_s}{\alpha_f}, \quad k^* = \frac{k_s}{k_f} \quad (\rho C_P)^* = \frac{(\rho C_P)_s}{(\rho C_P)_f}$$
(13)

Eqs. (1-5) are converted into the following dimensionless form;

$$\frac{\partial U}{\partial X} + \frac{\partial V}{\partial Y} = 0 \tag{14}$$

$$\frac{\partial U}{\partial \tau} + U \frac{\partial U}{\partial X} + V \frac{\partial U}{\partial Y} = -\frac{\partial P}{\partial X} + \left(\frac{\mu_{ff}}{\mu_{f}} \frac{\rho_{ff}}{\rho_{f}}\right) \Pr \left[2 \frac{\partial}{\partial X} \left(\mu_{a}^{*} \frac{\partial U}{\partial X}\right) + \frac{\partial}{\partial Y} \left(\mu_{a}^{*} \left(\frac{\partial U}{\partial Y} + \frac{\partial V}{\partial X}\right)\right)\right]$$
(15)

$$\frac{\partial V}{\partial \tau} + U \frac{\partial V}{\partial X} + V \frac{\partial V}{\partial Y} = -\frac{\partial P}{\partial Y} + \left(\frac{\mu_{ff}}{\mu_{f}} \frac{\rho_{ff}}{\rho_{f}}\right) \Pr \left[2 \frac{\partial}{\partial Y} \left(\mu_{a}^{*} \frac{\partial V}{\partial Y}\right) + \frac{\partial}{\partial X} \left(\mu_{a}^{*} \left(\frac{\partial U}{\partial Y} + \frac{\partial V}{\partial X}\right)\right)\right] \\
+ \left(\frac{(\rho \beta)_{ff}}{\rho_{ff} \beta_{f}}\right) Ra \Pr \theta_{ff} - \left(\frac{\sigma_{ff}}{\sigma_{f}} \frac{\rho_{f}}{\rho_{ff}}\right) Ha^{2} \Pr V$$
(16)

$$\frac{\partial \theta_{ff}}{\partial \tau} + U \frac{\partial \theta_{ff}}{\partial X} + V \frac{\partial \theta_{ff}}{\partial Y} = \left(\frac{\alpha_{ff}}{\alpha_f}\right) \left(\frac{\partial^2 \theta_{ff}}{\partial X^2} + \frac{\partial^2 \theta_{ff}}{\partial Y^2}\right), \text{ for the ferrofluid zone}$$
(17)

$$\frac{\partial \theta_s}{\partial \tau} = \alpha^* \left(\frac{\partial^2 \theta_s}{\partial R^2} + \frac{1}{R} \frac{\partial \theta_s}{\partial R} + \frac{\partial^2 \theta_s}{\partial Z^2} \right) + \frac{1}{(\rho C_P)^*} \frac{1}{A^*}, \text{ for the solid zone heat source}$$
 (18)

The dimensionless apparent viscosity is defined as follows;

$$\mu_a^* = \left\{ 2 \left[\left(\frac{\partial U}{\partial X} \right)^2 + \left(\frac{\partial V}{\partial Y} \right)^2 \right] + \left(\frac{\partial V}{\partial X} + \frac{\partial U}{\partial Y} \right)^2 \right\}^{\frac{n-1}{2}}$$
(19)

The initial and boundary conditions are;

$$\begin{array}{lll} \bullet & \tau = 0: U = V = 0, \; \theta_{f\!f} = 0.5, \; 0 \leq X \leq 1 \; \text{and} \; 0 \leq Y \leq \frac{1}{5} \\ \bullet & \tau > 0: U = V = 0, \; \theta_{f\!f} = 0.5, \; 0 \leq X \leq 1, \; Y = \frac{1}{5} \end{array}$$

•
$$\tau > 0 : U = V = 0, \ \theta_{ff} = 0.5, \ 0 \le X \le 1, \ Y = \frac{1}{5}$$

$$U = V = 0$$
, $\frac{\partial \theta_{ff}}{\partial y} = 0$, $0 \le Y \le \frac{1}{5}$, $X = 0$, $X = 1$ and $0 \le X \le 1$, $Y = 0$

$$U = V = 0$$
, $\frac{\partial \theta_f}{\partial n} = k^* \frac{\partial \theta_s}{\partial n}$, at the fluid – solid interface (20)

The Nusselt number around the perimeter of the heat-generating cylinder can be calculated by the following Eq. (21) [12, 50];

$$Nu(\theta) = \frac{k_{ff} \frac{\partial T_{ff}}{\partial n}}{k_f \frac{(T_{sf} - T_c)}{r}} = -\frac{k_{ff}}{k_f} \frac{1}{\theta_{sf}} \frac{\partial \theta_{ff}}{\partial n}$$
(21)

To find the average Nusselt number (Nu), we use the following integration;

$$Nu_{avg} = \frac{1}{2\pi} \int_{0}^{2\pi} Nu(\theta) d\theta$$
 (22)

3. Computation and validation

The numerical solution of the problem considered was carried out using the finite volume method with the SIMPLE algorithm developed by Patankar [51]. The dimensionless governing equations were discretized on a uniform staggered grid, adopting a curvilinear shape at the edges of the heating elements.

For the treatment of temporal and spatial terms, centered difference and QUICK schemes based on weighted quadratic interpolation were respectively adopted T. HAYASE et al. [52]. The iterative process was executed in a line-by-line procedure using the tri-diagonal matrix algorithm (TDMA). A time step of 10⁻³ was considered sufficiently accurate for this study. Acceptable error limits depend on the level of precision required for the study. A tolerance of 10⁻⁷ for residuals is used to ensure a converged and stable solution of the continuity, momentum and energy equations, and the convergence criterion for the sequential iterative solution was set by the following Eq. (23):

$$\frac{\sum_{i,j} \left| \phi_{i,j}^m - \phi_{i,j}^{m-1} \right|}{\sum_{i,j} \left| \phi_{i,j}^m \right|} \le 10^{-7}$$
 (23)

Here, ϕ represents variables U, V and θ , subscript (i, j) and exponent m denote spatial coordinates and number of iterations, respectively.

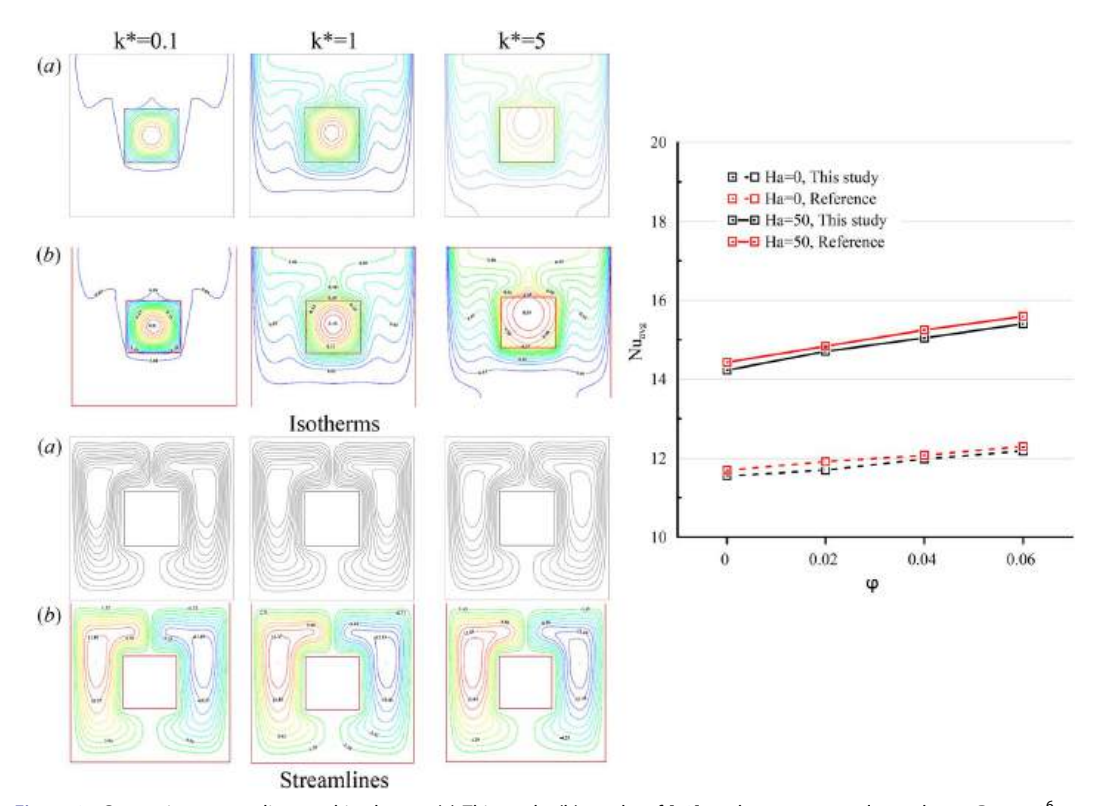


Figure 2. Comparison streamlines and isotherms. (a) This study, (b) results of [12], and average nusselt number at $Ra = 10^6$.

Table 2. Average nusselt number compared with data of L. Khezzar et al. [32].

n	Present study	Results [32]	Error %
0.6	7.2515	7.3823	1.7718
0.8	5.5703	5.6201	0.8861
1	4.6793	4.7662	1.8232
1.2	4.2021	4.2227	0.4878
1.4	3.8156	3.8464	0.8007

Table 3. Mesh sensitivity for Nu at Ra = 10^5 , Ha = 50, $k^* = 1$, n = 1. Nx =0.2, Ny = 0.1 and Nr = 0.056 (case 1).

Grid	61x13	101x21	141x29	181x37	221x45
Nu _{avg}	3.2016	3.1308	3.1292	3.1290	3.1290
$ heta_{max}$	0.5113	0.5007	0.4949	0.4947	0.4947

The bold values indicates that the 141x29 mesh has been chosen for this study.

To explore the problem formulated, it is important to ensure the accuracy of the existing code. To this end, a validation of the numerical data against those in the literature is unavoidable. To this end, a comparison of the isotherms, streamlines and average Nusselt number has been carried out with the data of S. Priyadharsini *et al.* [12] in the case of natural convection in a cavity filled with ferrofluid in the presence of a heat source presented in Figure 2. The mean Nusselt as a function of the power law index n in the case of natural convection of a cavity filled with a non-Newtonian fluid, has been compared with the results of L. Khezzar *et al.* [32], Table 2. These results show satisfactory agreement between our simulations and those in the literature.

Mesh sensitivity was also investigated using five grids 61×13 , 101×21 , 141×29 , 181×37 , and 221×45 . The maximum value of the dimensionless temperature and the average Nusselt number (Nu) were examined for each grid. The results presented in Table 3 show no essential differences between successive grids. Consequently, a 141×29 mesh is retained for all further calculations with optimal time.

4. Results and discussion

In this contribution, the cooling efficiency has been numerically studied, by transient natural thermomagnetic convection, of a long channel of aspect ratio N=0.2 equipped with four cylindrical heat-generating blocks with variable thermal conductivity. Ferrofluids consist of magnetite nano-additives suspended in a base fluid, which becomes strongly magnetized when an external magnetic field is applied, giving rise to thermogenic convection. The ferrofluid (Fe₃O₄) employed is considered to be non-Newtonian in character following the power law and $(\rho \text{Cp})^*=1$. The study was carried out for various geometric and thermophysical parameters. Different values of thermal conductivity (solid-fluid) (0.1 \leq k* \leq 10), power law index n (0.4 \leq n \leq 1.6), Rayleigh number ($10^4 \le \text{Ra} \le 10^7$), Hartmann number ($0 \le \text{Ha} \le 100$) and ferrofluid volume fraction ($0 \le \text{Ha} \le 100$) $\varphi \leq 0.1$), were considered. During this investigation, five geometric configuration cases were considered and studied. For this purpose, different ratios of shapes and positions of the heat-generating cylinders were defined. The first case consists of considering (Ny = 0.1 and Nr = 0.056), the second case (Ny = 0.12 and Nr = 0.056), the third case (Ny = 0.08 and Nr = 0.056), the fourth case (Ny = 0.1 and Nr = 0.028) and the fifth case (Ny = 0.1 and Nr = 0.085). For all cases, Nx = 0.2. The results will be illustrated in the form of streamlines, isotherms, average Nusselt number and a spatio-temporal characterization of the average ferrofluid velocity.

4.1. Effect on the thermal field

Figures 3–8, show isothermal and streamlines lines as a function of conductivity ratio k^* , power law flow index n and for two Hartmann number values (Ha = 0 and Ha = 100). Ferrofluid volume fraction and temperature gradient are fixed at $\varphi = 0.03$ and Ra = 10^5 , respectively. The figures show complex and interesting scenarios, highlighting the significant influence of control parameters on both isothermal and streamlines.

Moreover, since the boundary conditions are symmetrical, the results are symmetrical for all configurations. Furthermore, the homogeneous thermophysical properties of the Fe3O4 nanoparticles and the carrier fluid are essential in maintaining the symmetry. Since thermal conductivity, viscosity, and other properties are stated to maintain this uniformity (Eqs. 9–12) in the fluid,

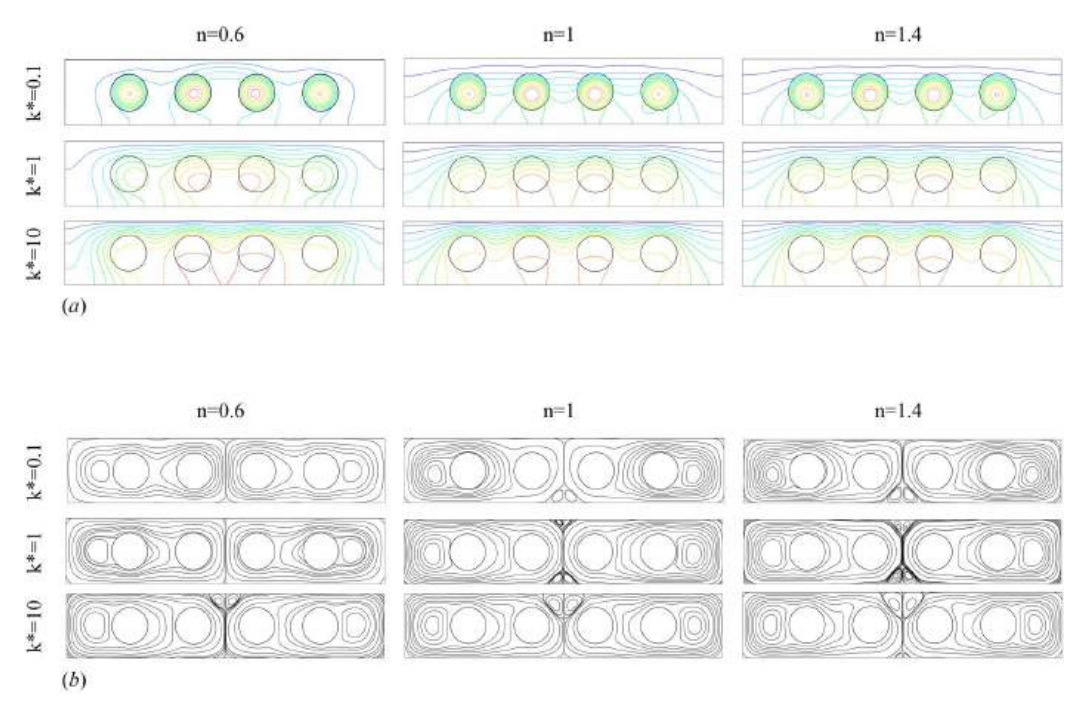


Figure 3. (a) Isotherms, (b) streamlines at Ha = 0, φ =0.03 and Ra = 10⁵ for various k* and n. Nx = 0.2, Ny = 0.1 and Nr = 0.056 (case 1).

temperature gradients and flow fields react in a consistent and balanced manner across the cavity. However, under specific cylindrical solid aspect ratio conditions, the symmetry may disappear. Indeed, this can be seen in result found for, $k^*=0.1$ and n=0.6. For this reason, the entire geometry was taken into account, rather than just half of it with symmetry about the vertical axis. For a low conductivity ratio ($k^*=0.1$), the thermal field is characterized by a concentration of isotherms on the heat-generating cylindrical blocks. This is due to the high thermal conductivity of the fluid relative to the solid. For $k^*=1$, a continuity of isothermal lines was observed for all cases, a consequence of the equality between fluid and solid conductivity. On the other hand, for $k^*=10$, on the other hand, isothermal lines appear to be concentrated on the fluid part of the geometry. These scenarios are valid for all types of fluid and all geometric configurations considered.

Figure 3, for a shear thinning pseudoplastic fluid (n=0.6) with low thermal conductivity (k*=0.1), the isothermal lines are rather less concentrated in the fluid zone and the heat source appears to be concentrated in the middle of the cylindrical solids. It is also important to note that the distortion of the isothermal lines for the case of a shear thinning pseudoplastic fluid indicates the signature of a convective transfer as a consequence of the low apparent viscosity of the non-Newtonian ferrofluid. As the index n increases, the lines widen from bottom to top and begin to intensify in the fluid zone, so the transfers show a conduction scenario for a shear thickening dilatant fluid. In addition, heat sources tend to move slightly downwards in the cavity. Clearly, as the apparent viscosity becomes greater, the transfers appear increasingly resistant and less pronounced, as a result of viscous dissipation, leading to a reduction in the ferrofluid's molecular agitation. For a conductivity ratio k* = 1, thermal stratification near the cold wall was found. Figure 3 shows that, for a pseudoplastic fluid, the heat source is more or less concentrated in the central part of the cylindrical blocks, tending downwards as the index n increases. An intense concentration of isotherms in the fluid zone is to be noted for high thermal conductivity.

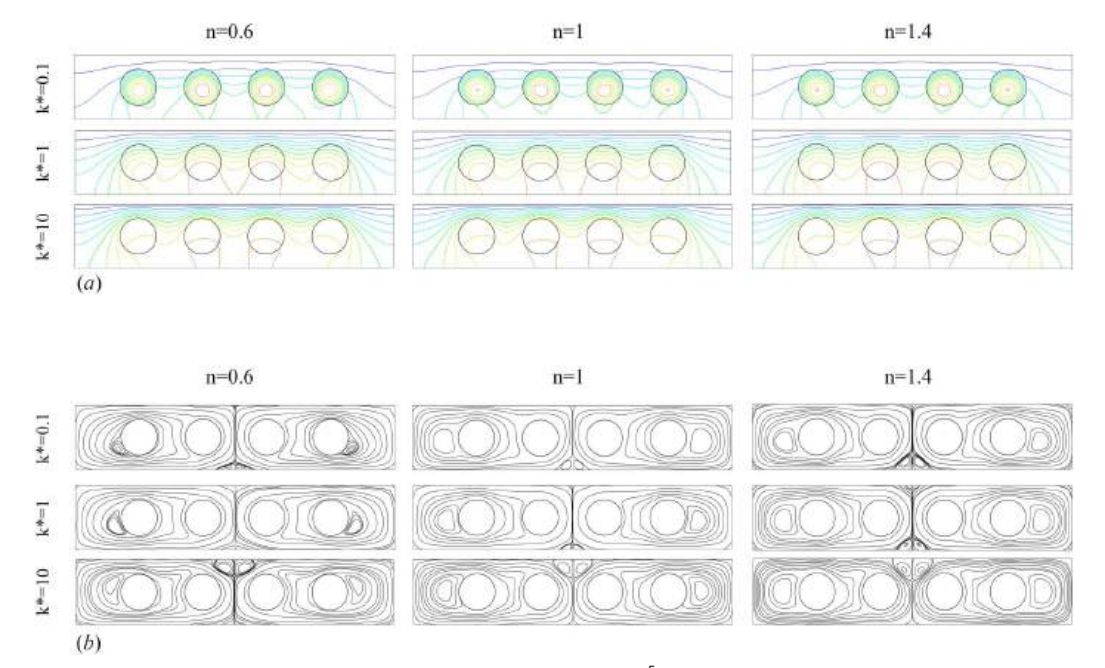


Figure 4. (a) Isotherms, (b) streamlines at Ha = 100, φ =0.03 and Ra = 10⁵ for various k* and n. Nx = 0.2, Ny = 0.1 and Nr = 0.056 (case 1).

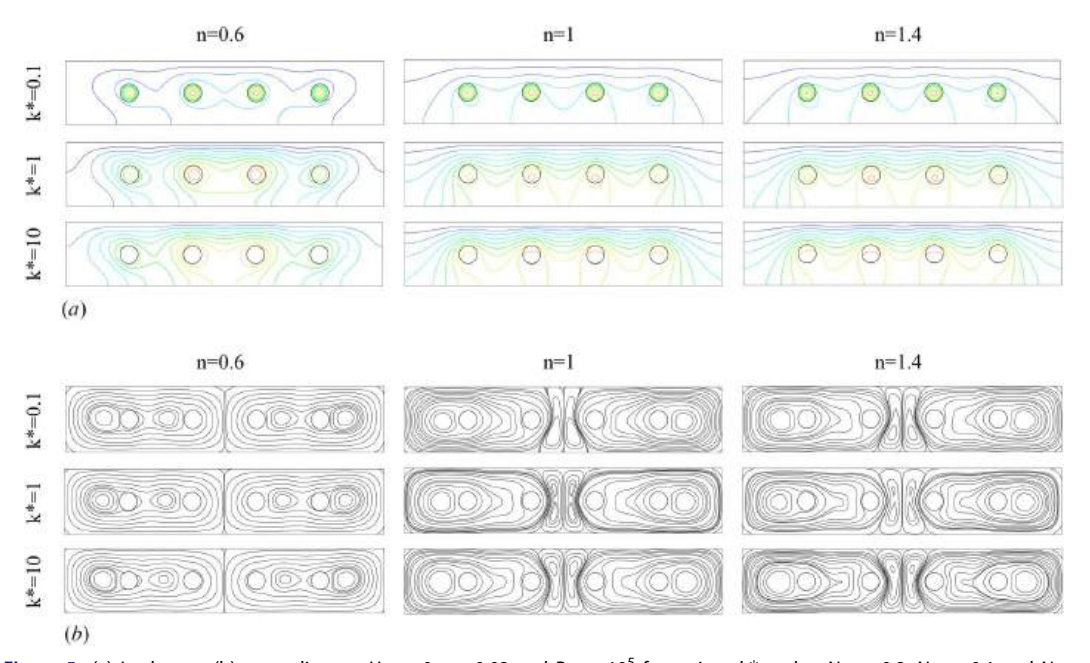


Figure 5. (a) Isotherms, (b) streamlines at Ha = 0, φ =0.03 and Ra = 10⁵ for various k* and n. Nx = 0.2, Ny = 0.1 and Nr = 0.028 (Case 4).

In fact, no change was observed for either a Newtonian or a dilatant fluid. Furthermore, when the thermal field is subjected to an external magnetic force, the isothermal lines appear to be affected by the Hartmann number (Ha = 100), Figure 4. Although the magnetic force acting on the Fe3O4 nanoparticles is oriented in the x direction, the resulting Lorentz forces are

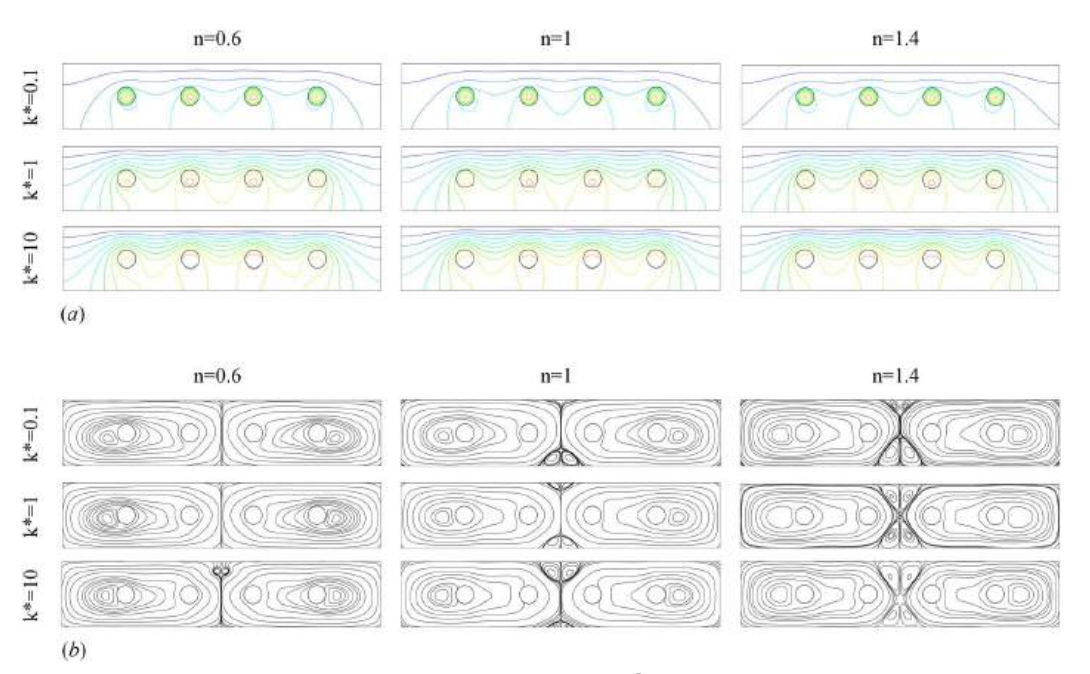


Figure 6. (a) Isotherms, (b) streamlines at Ha = 100, φ =0.03 and Ra = 10⁵ for various k* and n. Nx = 0.2, Ny = 0.1 and Nr = 0.028 (case 4).

symmetrically distributed due to the uniform distribution of the nanoparticles and the symmetry of the initial conditions. Thus, the net effect on the temperature and flow fields can remain symmetrical. For all values of thermal conductivity, practically the same isotherms structures can be observed with the disappearance of the hot-source cell for a Newtonian fluid with $k^*=1$.

The thermal field shown in Figure 5, for the fourth case (Nx = 0.2, Ny = 0.1, Nr = 0.028), exhibits similar patterns in the isothermal lines. However, with the exception of the case with conductivity $k^* = 1$, here the heat source cell occupies the interior of the solid and tends to move downwards as the index n increases. A layered arrangement of isotherms in the vicinity of the cold wall can be seen when the index n and the conductivity ratio become important. In Figure 6, under the application of a high-intensity magnetic field (Ha = 100), the isothermal lines display a tendency to decelerate, with power-law invariance as a function of the index n. All these results show symmetrical structures. In contrast, Figure 7 shows a different scenario when increasing the cylinder aspect ratio (Nx = 0.2, Ny = 0.1, Nr = 0.085). For low thermal conductivity, in the case of a pseudoplastic fluid (n = 0.6), the isothermal lines show asymmetry, resulting from the size of the cylinders considered in this particular case, which generate heat and exert resistance to its diffusion into the fluid zone. On the other hand, in Figure 8, as the magnetic field increases (Ha = 100), the isothermal lines regain their symmetry when the heat source disappears for $k^* = 1$, resulting from the transfer resistance induced by the magnetic force.

4.2. Effect on the flow field

The flow field shown in Figure 3 shows that streamlines are characterized by the formation of two large contra-rotating cells that are symmetrical with respect to the vertical axis. In fact, due to the presence of the cylindrical blocks, areas of flow stagnation were observed on both the right and left sides of the cavity. In these areas, the flow is blocked by the cylinders, resulting in the formation of two secondary cells. On the other hand, as the index n increases, secondary cells are

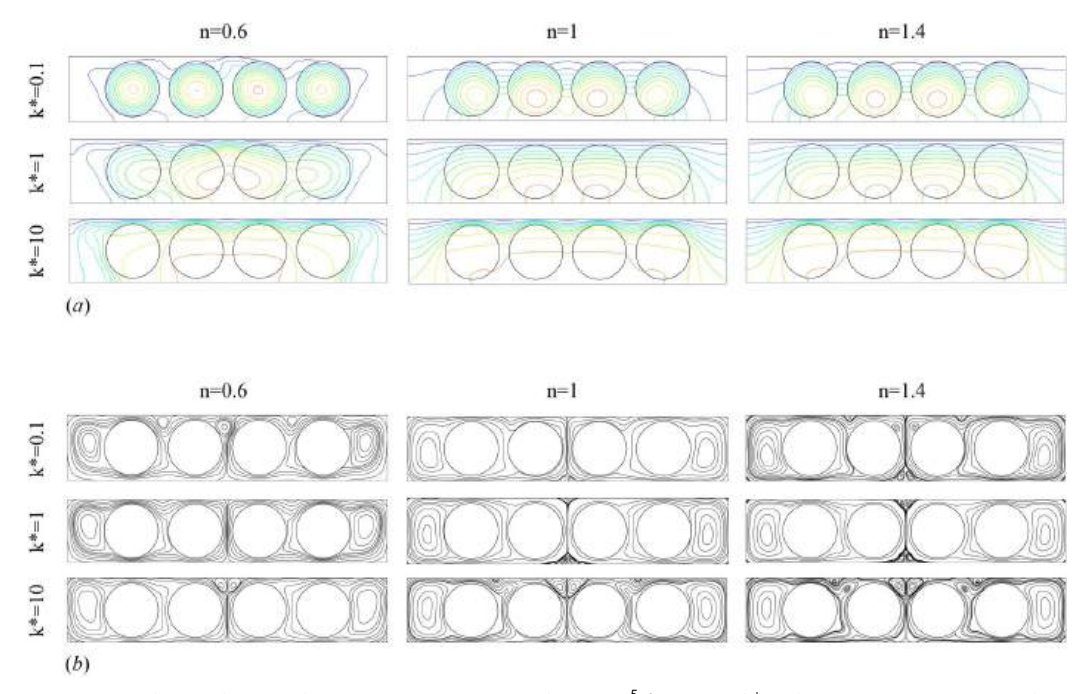


Figure 7. (a) Isotherms, (b) streamlines at Ha = 0, φ =0.03 and Ra = 10⁵ for various k* and n. Nx = 0.2, Ny = 0.1 and Nr = 0.085 (case 5).

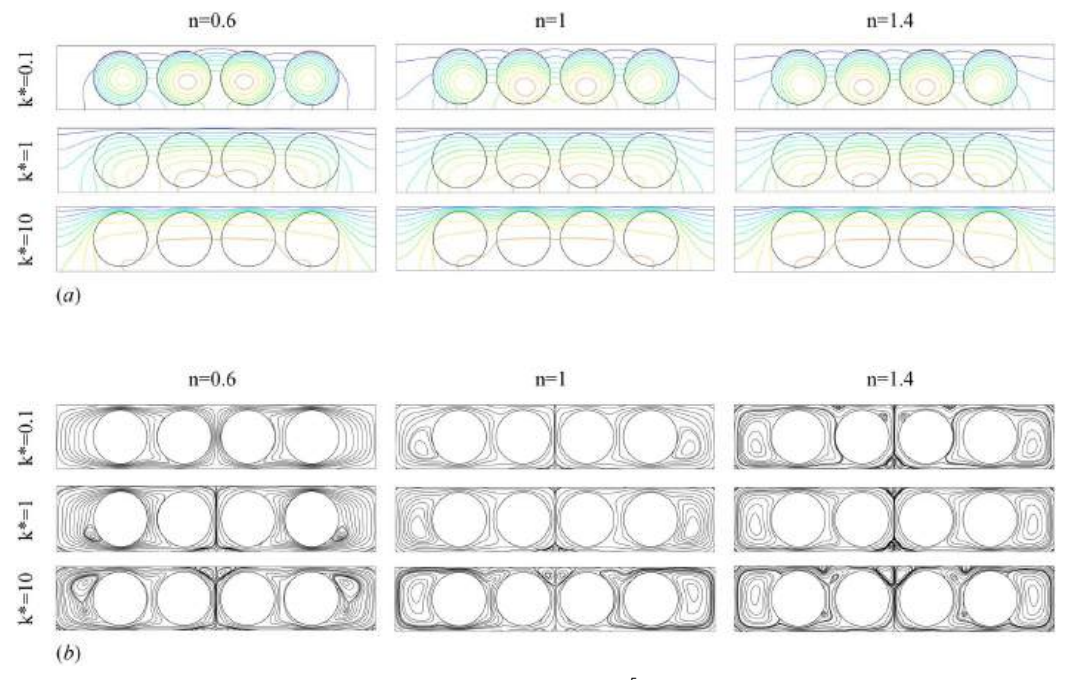


Figure 8. (a) Isotherms, (b) streamlines at Ha = 100, φ =0.03 and Ra = 10⁵ for various k* and n. Nx = 0.2, Ny = 0.1 and Nr = 0.085 (case 5).

generated. When $k^* = 0.1$ and $k^* = 1$, two small cells are born in the middle of the bottom wall, with a particularity for $k^*=1$ and n=1.4. In this situation, we see the formation of four secondary cells, two in the middle of the high wall and two in the middle of the low wall. On the other hand, for high thermal conductivity k*=10, all streamlines are characterized by two main cells with stagnation regions to the left and right, and two secondary cells formed in the middle of the top wall. The intensity of these secondary cells increases as the power law index n increases. Clearly, increasing the power law index n leads to the formation of secondary cells, resulting in a reduced flow field. This outcome can be attributed to the non-Newtonian nature of a dilatant ferrofluid (n > 1), wherein viscosity rises with shear rate, consequently leading to an increase of the stagnation regions.

In Figure 4, as the Hartmann number increases to 100, the cells undergo flattening and elongation primarily along the horizontal axis within the cavity. This phenomenon underscores the substantial magnetic reactivity of the ferrofluid subjected to an external magnetic field. The suspended magnetic particles within the fluid react by aligning themselves with the magnetic field lines, enabling the ferrofluid to behave magnetically. For a pseudoplastic ferrofluid with low thermal conductivity, the stagnation zone near the left and right cavity walls is reduced. In fact, the flow is characterized by two large main cells and two secondary cells, which are disappearing in the stagnation zones. Moreover, this disappearance will induce the creation of other secondary cells near the middle of the lower wall for conductivities $k^*=0.1$ and $k^*=1$. In the case of $k^*=10$, the cells formed in the stagnation zones tend to overcome the buoyancy forces and begin to move toward the upper part of the two cylinders on the left and right.

Changing the aspect ratio of the cylinders, as depicted in Figure 5, leads to the formation of further stagnation zones. To this end, the scenario shown in this figure is bicellular for a pseudoplastic fluid, marked by the emergence of four secondary cells near the stagnation zones. For a Newtonian fluid and a dilatant fluid, the flow is characterized by four rotating contra cells symmetrical to the horizontal axis of the cavity. Moreover, for low thermal conductivity, the nuclei of the two cells formed in the middle of the cavity lie close to the low wall, and the intensity of these nuclei tends to overcome buoyancy forces as the conductivity ratio becomes larger, so the cells move increasingly toward the high wall. As the Hartmann number increases, Figure 6 shows the separation of the two cells formed in the middle of the cavity, leading to the emergence of additional symmetrical, contra-rotating cells. Indeed, the flow intensity is relatively low as a result of the Lorentz force driven by a magnetic field.

Figures 7 and 8 show the streamlines for a large-cylinder aspect ratio. From the results presented in these figures, we can see that a dissymmetry has just appeared for a pseudoplastic fluid (n=0.6) of low thermal conductivity, so the flow is characterized by two large main cells with the formation of three other secondary cells resulting in the creation of stagnation zones when the aspect ratio of the cylinders becomes large. In addition, the application of a magnetic field reduces the flow intensity and the structure of the iso-current lines becomes symmetrical again.

4.3. Effect on heat transfer rate

Figure 9, shows the evolution of the average Nusselt number along the perimeters of the four heat-generating cylinders as a function of the index n for different thermal conductivities, Ha =0, Ra = 10^5 and $\varphi = 0.03$. The results show that efficient transfer is found for a pseudoplastic fluid (n < 1) of low thermal conductivity for all cases. Thus, the Nusselt profiles show an almost constant evolution for a Newtonian and dilatant fluid. Clearly, this is due to the impact of the apparent viscosity of the ferrofluid as the power law index n becomes more important. It is also important to note that the effect of the conductivity ratio is inversely proportional to the power law index n for all geometrical configurations, except for case 2 and case 5. The figures show that for high conductivity, the transfer rate is rather pronounced for Newtonian and dilatant fluids.

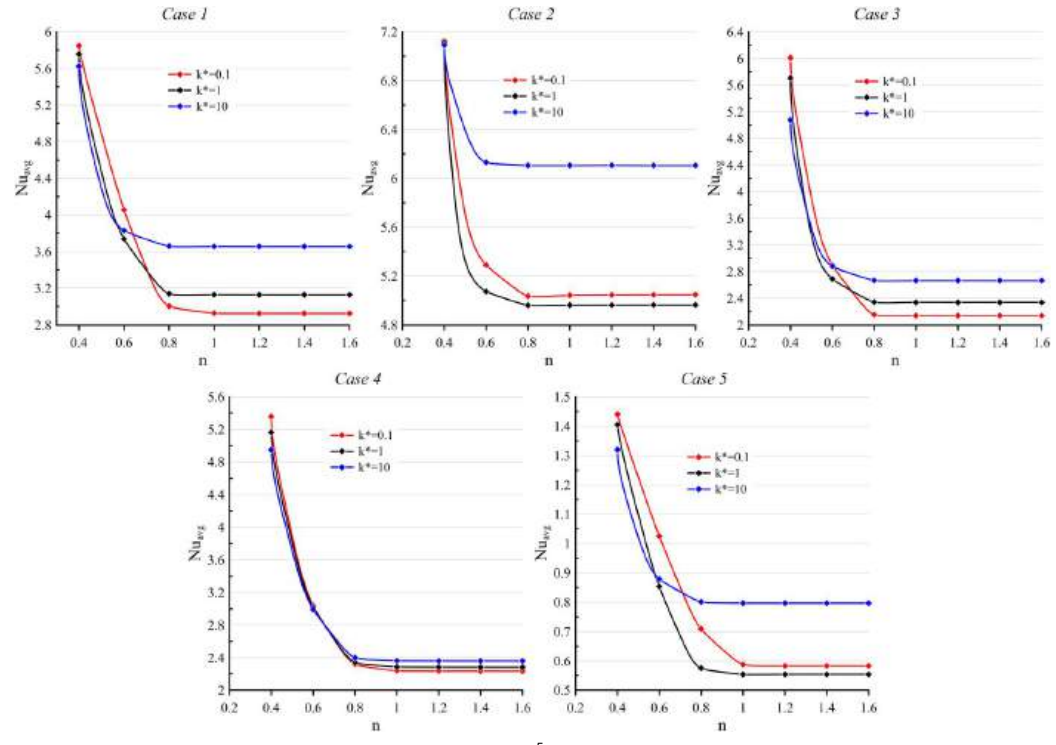


Figure 9. Average Nusselt as a function of n for Ha = 0 $Ra = 10^5$.

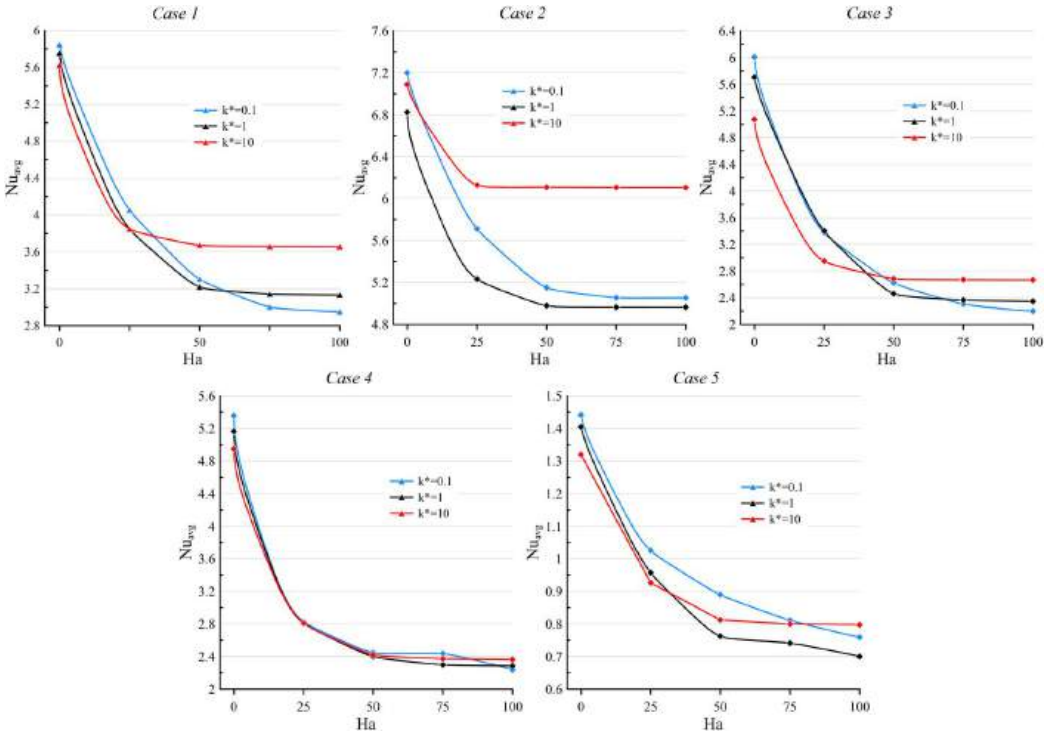


Figure 10. Average Nusselt as a function of Ha and k^* for n = 0.4 Ra $= 10^5$.

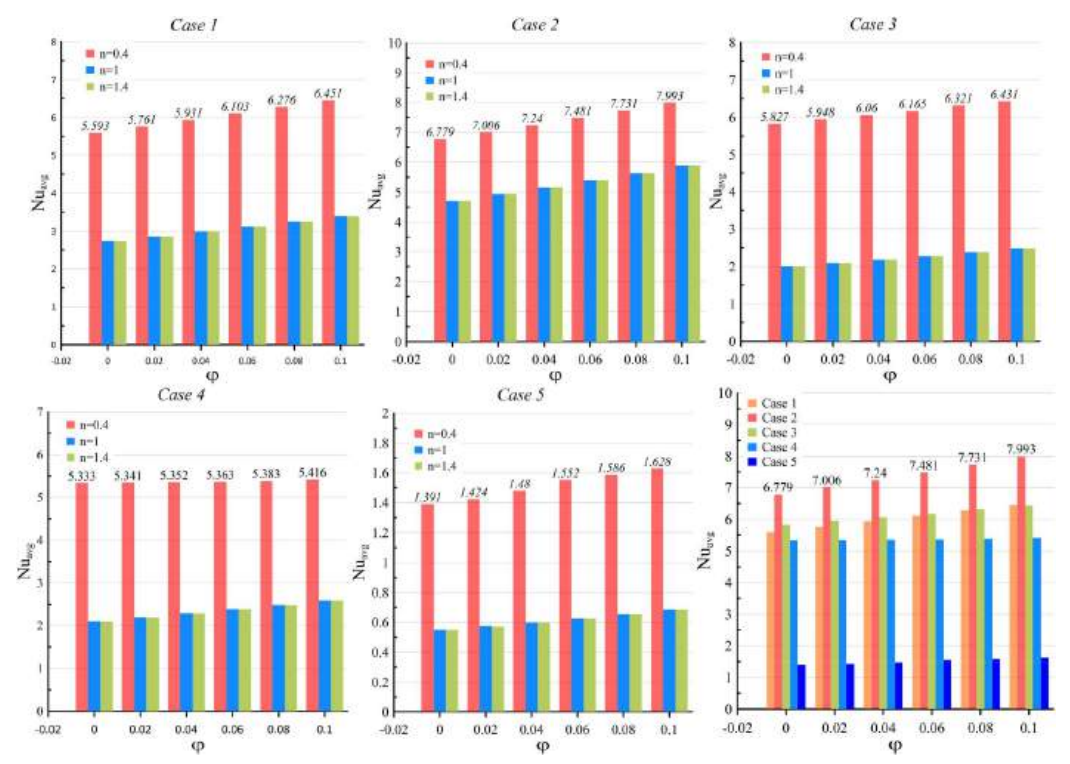


Figure 11. Average Nusselt as a function of φ for Ra = 10⁵, k*=0.1 and Ha = 0.

Figure 10 shows the evolution of the average Nusselt number of a pseudoplastic fluid (n = 0.4) as a function of the Hartmann number for different values of thermal conductivity. It can be seen that the heat transfer rate is a decreasing function of the Hartmann number. Furthermore, we can see that effective cooling is found in the low thermal conductivity of the ferrofluid.

In order to further increase convective transfer and achieve optimum cooling of the thermal system under consideration, additional quantities of nano-sized iron oxide additives were added to the base fluid. To this end, Figure 11, shows the evolution of the average Nusselt number as a function of the ferrofluid volume fraction for all cases considered and for all types of ferrofluids in the case of a fixed thermal conductivity, k*=0.1. The results presented in these figures show that heat transfer increases linearly with the addition of nanoparticles. According to these figures, a pseudoplastic ferrofluid with index n = 0.4 can greatly enhance heat transfer. For Case 4, on the other hand, the rate of heat transfer appears to be substantially constant with the addition of nanoparticles. The results show that the heat transfer rate is improved by 7.62% for case 1, 15.19% for case 2, 9.39% for case 3, 1.53% for case 4 and 14.55% for case 5. Furthermore, the results show that maximum transfer can be achieved for case 2 when the cylindrical blocks are close to the cold wall with aspect ratios Nx = 0.2, Ny = 0.12 and Nr = 0.056. And, a minimum heat transfer is obtained for case 5 when the cylinders are large with aspect ratios Nx = 0.2, Ny = 0.1 and Nr = 0.085, indicating that cooling is improved by 79.63% between case 2 and case 5 using a pseudoplastic ferrofluid with a low thermal conductivity.

The effect of the temperature gradient on the Nusselt number for different values of index n, Hartmann number and thermal conductivity ratio is illustrated in Figure 12. Nusselt profiles as a function of index n follow an exponential law for different values of Rayleigh number. Heat transfer can be enhanced by increasing the temperature gradient, particularly for pseudoplastic fluids with low thermal conductivity ($k^*=0.1$). For low values of Rayleigh number, the transfer appears invariant as a function of the power law index n, and the Nusselt profile is almost

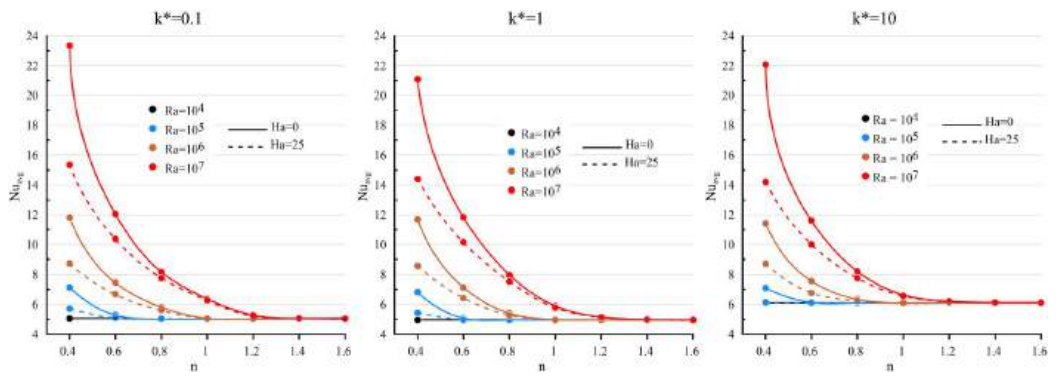


Figure 12. Average Nusselt as a function of n for n = 0.4 and Ha = 0 and $k^* = 0.1$. Case 2.

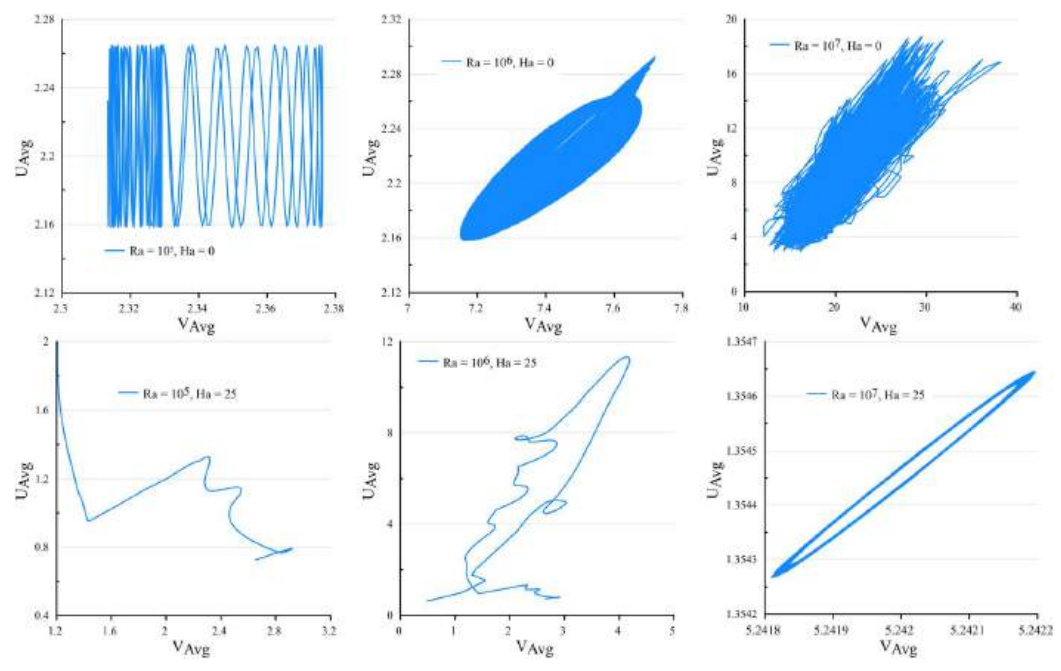


Figure 13. Phase portrait of average velocity as a function of Ra and Ha for n = 0.4 and k = 0.1. Case 2.

constant. Furthermore, all Nusselt number profiles converge toward a common limit as the index n increases. We can therefore conclude that dilatant fluids with an index $(n \ge 1.2)$ are not influenced by either Rayleigh or Harmann numbers. Indeed, ferrofluid can be used to regulate temperature in a thermal system.

To this end, Figure 13 shows the phase portraits of the mean velocity as a function of the Rayleigh number and Hartmann number of a pseudoplastic ferrofluid with index n = 0.4 and conductivity $k^*=0.1$. It's important to look at the spatiotemporal evolution of the ferrofluid velocity, because at large temperature gradients we can have an efficient transfer rate, but this can have a negative impact on the thermal system under consideration, leading to major consequences and failure. For example, when the Rayleigh number $R=10^7$ and $Ra=10^6$, the transfer shown in Figure 12 appears to be very efficient, but if we look at Figure 13, the phase portrait shows unstable regimes whose evolutions are chaotic and unpredictable. On the other hand, when $Ra=10^5$, the space-time attraction of the velocities shows a quasi-periodic regime, so the dynamics of the system seems to become increasingly stable as the Rayleigh number decreases.

Of particular interest is the potential effect of the application of an external magnetic field on high temperature gradients in the system. To this end, applying and increasing the Hartmann number can stabilize the system, thereby reducing chaotic phenomena. When $Ra = 10^7$ and Ha = 25, the dynamics shown in this figure are stable, with the attraction of a thick limit cycle being predictable. As the Rayleigh number decreases, while maintaining the same magnetic field strength (Ha = 25), we see a stabilization of average velocities in the channel. Indeed, for Ra = 10^6 and Ra = 10^5 , the phase portraits show a dynamic of a limit point, so the regime appears increasingly stable for low temperature gradients. On the other hand, what is of real interest is when the Rayleigh number is very large, as the dynamics become increasingly stable as the Hartmann number increases. To this end, the application of a magnetic field for cooling a thermal system is crucial, because at some point, the rate of heat transfer must be reduced to avoid any kind of long-term process malfunction. Indeed, the application of a magnetic field of intensity Ha = 25 can lead to flow stabilization and convective transfers of pseudoplastic ferrofluids.

5. Conclusion

This study presents an analysis of transient natural convection cooling of a channel with aspect ratio N=0.2, long enough for the system to reduce to 2D, equipped with four cylindrical heatgenerating blocks. The main objective of this study is to analyze the effect of magnetic field, temperature gradient, aspect ratio and position of the heat-generating blocks on transient natural convection, also taking into account variations in heat-generating block thermal conductivity, power law index n and nanoparticle volume fraction. The results were illustrated in the form of streamlines, isotherms, mean Nusselt number profiles and a spatio-temporal characterization of the mean ferrofluid velocity. Heat transfer and flow are largely influenced by variations in the control parameters, indicating that increasing the apparent viscosity of the ferrofluid reduces heat transfer and the flow field. Thus, the flow is characterized by strong circulation for pseudoplastic fluids and weak circulation for Newtonian and dilatant fluids. Furthermore, heat transfer appears to be dominated by natural convection in the case of pseudoplastic fluids, tending toward conduction as the index n increases. As for the effect of the thermal conductivity ratio (fluid-solid), the results show that effective cooling can be recovered for a low thermal conductivity $k^*=0.1$. In addition, the addition of additional iron oxide nano-additives to the base fluid can also enhance convective transfer in the thermal system under consideration. During the investigation, it was observed that, when using a system with an aspect ratio (Ny = 0.12 and Nr = 0.056), which corresponds to case 2, maximum transfer can be recovered.

From an energy-saving point of view, this configuration can provide a good approximation for selecting effective physical and geometrical parameters to design a reliable thermal system. To this end, we can conclude that the choice of non-Newtonian ferrofluid of pseudo plastic type having a low thermal conductivity ratio subjected to a uniform magnetic field proves to be a crucial solution for effective cooling of a long channel equipped with cylindrical blocks generating heat.

Based on the different parameters studied in this research and the results obtained, scenarios linking these study parameters could easily be used in the design and optimization of several thermal engineering problems related to heat exchangers. Subsequently, it would be interesting to complete this study by including thermal damping parameters, such as the application of an external magnetic field, with the aim of minimizing heat loss to the external environment. It would also be interesting to link the magnetic field to the non-Newtonian behavior of a hybrid nanofluid consisting of solids immersed in a magnetorheological fluid.

Disclosure statement

The authors declare that they have no known competing financial interests or personal relationships that could have appeared to influence the work reported in this article.

ORCID

Massinissa Adnani http://orcid.org/0000-0001-7099-8409
Adel Sahi http://orcid.org/0000-0001-5629-7761
Bachir Meziani http://orcid.org/0000-0003-1845-0619
Abdelhakim Benslimane http://orcid.org/0000-0002-6554-6309
Ali J. Chamkha http://orcid.org/0000-0002-8335-3121

References

- [1] A. J. Chamkha and M. A. Ismael, "Natural convection in differentially heated partially porous layered cavities filled with a nanofluid," *Numerical Heat Transfer, Part A Appl.*, vol. 65, no. 11, pp. 1089–1113, 2014. DOI: 10.1080/10407782.2013.851560.
- [2] Y. Tizakast, M. Kaddiri, M. Lamsaadi and T. Makayssi, "Machine learning based algorithms for modeling natural convection fluid flow and heat and mass transfer in rectangular cavities filled with non-Newtonian fluids," *Eng. Appl. Artif. Intell.*, vol. 119, pp. 105750, 2023. DOI: 10.1016/j.engappai.2022.105750.
- [3] L. C. Ngo, T. Bello-Ochende and J. Meyer, "Numerical investigation of natural convection of cavity receiver for low power application," *Int. J. Green Energy*, vol. 13, no. 8, pp. 845–851, 2016. DOI: 10.1080/15435075. 2016.1161628.
- [4] J. Xiong, G. Mao and Y. Zhang, "Numerical computation on cavity natural convection for built-in plate arrays application: heat transfer analysis and optimization," *Numer. Heat Transfer Part A Appl.*, pp. 1–20, 2023. DOI: 10.1080/10407782.2023.2278704.
- [5] S.-K. Choi, S.-O. Kim, T.-H. Lee and Dohee-Hahn, "Computation of the natural convection of nanofluid in a square cavity with homogeneous and nonhomogeneous models," *Numer. Heat Transfer Part A Appl.*, vol. 65, no. 4, pp. 287–301, 2014. DOI: 10.1080/10407782.2013.831695.
- [6] D. Mansoury, F. I. Doshmanziari, A. Kiani, A. J. Chamkha and M. Sharifpur, "Heat transfer and flow characteristics of Al2O3/water nanofluid in various heat exchangers: experiments on counter flow," *Heat Transfer Eng.*, vol. 41, no. 3, pp. 220–234, 2020. DOI: 10.1080/01457632.2018.1528051.
- [7] L. Snoussi, N. Ouerfelli, X. Chesneau, A. J. Chamkha, F. B. M. Belgacem and A. Guizani, "Natural convection heat transfer in a nanofluid filled U-shaped enclosures: numerical investigations," *Heat Transfer Eng.*, vol. 39, no. 16, pp. 1450–1460, 2018. DOI: 10.1080/01457632.2017.1379343.
- [8] M. Mokaddes Ali, R. Akhter and M. A. Alim, "Hydromagnetic natural convection in a wavy-walled enclosure equipped with hybrid nanofluid and heat generating cylinder," *Alexand. Eng. J.*, vol. 60, no. 6, pp. 5245–5264, 2021. DOI: 10.1016/j.aej.2021.04.059.
- [9] M. Boukendil, L. El Moutaouakil, Z. Zrikem and A. Abdelbaki, "Natural convection and surface radiation in an insulated square cavity with inner hot and cold square bodies," *Mater. Today Proc.*, vol. 45, pp. 7282–7289, 2021. DOI: 10.1016/j.matpr.2020.12.1011.
- [10] M. Foruzan Nia, A. B. Ansari and S. A. Gandjalikhan Nassab, "Transient combined volumetric radiation and free convection in a chamber with a hollow heat-generating solid body," *Int. Commun. Heat Mass Transfer*, vol. 119, pp. 104937, 2020. DOI: 10.1016/j.icheatmasstransfer.2020.104937.
- [11] C. Sivaraj, E. Vignesh and M. A. Sheremet, "Thermogravitational convection of ferrofluid combined with the second law of thermodynamics for an open chamber with a heat-generating solid block under an influence of uniform magnetic field," *Int. Commun. Heat Mass Transfer*, vol. 129, pp. 105712, 2021. DOI: 10. 1016/j.icheatmasstransfer.2021.105712.
- [12] S. Priyadharsini and C. Sivaraj, "Numerical simulation of thermo-magnetic convection and entropy production in a ferrofluid filled square chamber with effects of heat generating solid body," *Int. Commun. Heat Mass Transfer*, vol. 131, pp. 105753, 2022. DOI: 10.1016/j.icheatmasstransfer.2021.105753.
- [13] A. Sahi, M. Hamdi, D. Sadaoui, B. Meziani and O. Ourrad, "Effect of MHD mixed convection on a heat-generating element cooling inside a ventilated square cavity filled with Fe3O4-water ferrofluid," *Numer. Heat Transfer Part A Appl.*, vol. 84, no. 8, pp. 837–852, 2023. DOI: 10.1080/10407782.2022.2163943.
- [14] D. Khan, G. Ali, P. Kumam and P. Suttiarporn, "A generalized electro-osmotic MHD flow of hybrid ferro-fluid through Fourier and Fick's law in inclined microchannel," *Numer. Heat Transfer Part A Appl.*, vol. 85, no. 18, pp. 3091–3109, 2023. DOI: 10.1080/10407782.2023.2232535.



- A. Vatani, P. L. Woodfield, N.-T. Nguyen and D. V. Dao, "Onset of thermomagnetic convection around a vertically oriented hot-wire in ferrofluid," J. Magnetism Magn. Mater., vol. 456, pp. 300-306, 2018. DOI: 10.1016/j.jmmm.2018.02.040.
- [16] M. Bahiraei, M. Hangi and A. Rahbari, "A two-phase simulation of convective heat transfer characteristics of water-Fe3O4 ferrofluid in a square channel under the effect of permanent magnet," APPl. Thermal Eng., vol. 147, pp. 991–997, 2019. DOI: 10.1016/j.applthermaleng.2018.11.011.
- [17] S. O. Giwa, M. Sharifpur and J. P. Meyer, "Effects of uniform magnetic induction on heat transfer performance of aqueous hybrid ferrofluid in a rectangular cavity," APPI. Therm Eng., vol. 170, pp. 115004, 2020. DOI: 10.1016/j.applthermaleng.2020.115004.
- [18] S. Saranya, L. Baranyi and Q. M. Al-Mdallal, "Free convection flow of hybrid ferrofluid past a heated spinning cone," Thermal Sci. Eng. Prog., vol. 32, pp. 101335, 2022. DOI: 10.1016/j.tsep.2022.101335.
- [19] Y. Cao, et al., "Heat transfer analysis on ferrofluid natural convection system with magnetic field," Ain Shams Eng. J., vol. 14, no. 9, pp. 102122, 2023. DOI: 10.1016/j.asej.2023.102122.
- [20] E. Gürsoy, et al., "Effect of magnetic field locations on thermo-magnetic convection performance of Fe3O4/ H2O ferrofluid flowing in a novel dimpled tube: an experimental study," Appl. Thermal Eng., vol. 226, pp. 120305, 2023. DOI: 10.1016/j.applthermaleng.2023.120305.
- [21] B. Iftikhar, M. Arshad Siddiqui and T. Javed, "Dynamics of magnetohydrodynamic and ferrohydrodynamic natural convection flow of ferrofluid inside an enclosure under non-uniform magnetic field," Alexand. Eng. J., vol. 66, pp. 523–536, 2023. DOI: 10.1016/j.aej.2022.11.011.
- [22] M. Nemati, M. Sefid, A. Karimipour and A. J. Chamkha, "Computational thermal performance analysis by LBM for cooling a hot oval object via magnetohydrodynamics non-Newtonian free convection by using magneto-ferrofluid," J. Magnetism Magnetic Mater., vol. 577, pp. 170797, 2023. DOI: 10.1016/j.jmmm.2023.
- [23] K. Gangadhar, D. Vijayakumar, A. J. Chamkha, T. Kannan and G. Sakthivel, "Effects of newtonian heating and thermal radiation on micropolar ferrofluid flow past a stretching surface: spectral quasi-linearization method," Heat Trans., vol. 49, no. 2, pp. 838-857, 2019. DOI: 10.1002/htj.21641.
- A. Kongassery, et al., "Morphological effects on natural convection heat transfer of magnesium ferrite ferrofluid," Heat Transfer Eng., vol. 45, no. 10, pp. 892-903, 2024. DOI: 10.1080/01457632.2023.2227806.
- [25] K. Khellaf and G. Lauriat, "Numerical study of heat transfer in a non-Newtonian Carreau-fluid between rotating concentric vertical cylinders," J. Non-Newtonian Fluid Mech., vol. 89, no. 1-2, pp. 45-61, 2000. DOI: 10.1016/S0377-0257(99)00030-0.
- [26] H. Demir and F. T. Akyõldõz, "Unsteady thermal convection of a non-Newtonian fluid," Int. J. Eng. Sci., vol. 38, no. 17, pp. 1923–1938, 2000. DOI: 10.1016/S0020-7225(00)00011-2.
- [27] Z. Alloui and P. Vasseur, "Natural convection of Carreau-Yasuda non-Newtonian fluids in a vertical cavity heated from the sides," Int. J. Heat Mass Transfer., vol. 84, pp. 912-924, 2015. DOI: 10.1016/j.ijheatmasstransfer.2015.01.092.
- [28] A. Boutra, A. Bourada and Y. K. Benkahla, "Free convection of Ostwald-de Waele fluid within square enclosure equipped with heat-generating circular solid: MRT-LBM simulation," J. Taiwan Inst. Chem. Eng., vol. 149, pp. 104999, 2023. DOI: 10.1016/j.jtice.2023.104999.
- R. R. Kairi and P. V. S. N. Murthy, "Effect of viscous dissipation on natural convection heat and mass [29] transfer from vertical cone in a non-Newtonian fluid saturated non-Darcy porous medium," APPI. Mathematics Computation, vol. 217, no. 20, pp. 8100-8114, 2011. DOI: 10.1016/j.amc.2011.03.013.
- [30] S. Yigit, M. Battu, O. Turan and N. Chakraborty, "Free convection of power-law fluids in enclosures with partially heating from bottom and symmetrical cooling from sides," Int. J. Heat Mass Transfer., vol. 145, pp. 118782, 2019. DOI: 10.1016/j.ijheatmasstransfer.2019.118782.
- [31] M. Ghalambaz, S. M. Hashem Zadeh, S. A. M. Mehryan, K. Ayoubi Ayoubloo and N. Sedaghatizadeh, "Non-Newtonian behavior of an electrical and magnetizable phase change material in a filled enclosure in the presence of a non-uniform magnetic field," Int. Commun. Heat Mass Transfer., vol. 110, pp. 104437, 2020. DOI: 10.1016/j.icheatmasstransfer.2019.104437.
- [32] L. Khezzar, D. Siginer and I. Vinogradov, "Natural convection of power law fluids in inclined cavities," Int. J. Thermal Sci., vol. 53, pp. 8-17, 2012. DOI: 10.1016/j.ijthermalsci.2011.10.020.
- H. Zeb, H. A. Wahab, U. Khan and A. J. Chamkha, "Magnetic dipole effects on non-Newtonian ferrofluid [33] over a stretching sheet," Heat Trans., vol. 52, no. 1, pp. 759-779, 2022. DOI: https://onlinelibrary.wiley. com. / DOI: 10.1002/htj.22715.
- [34] A. M. Rashad, M. A. El-Hakiem and M. M. M. Abdou, "Natural convection boundary layer of a non-Newtonian fluid about a permeable vertical cone embedded in a porous medium saturated with a nanofluid," Comput. Math. Appl., vol. 62, no. 8, pp. 3140-3151, 2011. DOI: 10.1016/j.camwa.2011.08.027.
- [35] P. P. Roy, S. Chowdhury, M. H. Raj, M. Q. Islam and S. Saha, "Forced, natural and mixed convection of Non-Newtonian fluid flows in a square chamber with moving lid and discrete bottom heating," Res. Eng., vol. 17, pp. 100939, 2023. DOI: 10.1016/j.rineng.2023.100939.

- [36] Z. M. Agool and R. H. Hameed, "Experimental investigation of heat transfer with natural convection of non-newtonian fluid inside the enclosure with hot obstacle," *Mater. Today Proc.*, vol. 61, pp. 892–900, 2022. DOI: 10.1016/j.matpr.2021.10.039.
- [37] C. Sasmal and R. P. Chhabra, "Laminar natural convection from a heated square cylinder immersed in power-law liquids," *J. Non-Newtonian Fluid Mechanics*, vol. 166, no. 14-15, pp. 811–830, 2011. DOI: 10. 1016/j.jnnfm.2011.04.013.
- [38] N. O. Moraga, G. P. Parada and D. A. Vasco, "Power law non-Newtonian fluid unsteady conjugate three-dimensional natural convection inside a vessel driven by surrounding air thermal convection in a cavity," *Int. J. Thermal Sci.*, vol. 107, pp. 247–258, 2016. DOI: 10.1016/j.ijthermalsci.2016.04.007.
- [39] T. Sarala Devi, C. Venkata Lakshmi, K. Venkatadri and M. Suryanarayana Reddy, "Influence of external magnetic wire on natural convection of non-Newtonian fluid in a square cavity," *Partial Differential Equat. APPL. Mathem.*, vol. 4, pp. 100041, 2021. DOI: 10.1016/j.padiff.2021.100041.
- [40] D. S. Loenko, A. Shenoy and M. A. Sheremet, "Effect of time-dependent wall temperature on natural convection of a non-Newtonian fluid in an enclosure," *Int. J. Thermal Sciences*, vol. 166, pp. 106973, 2021. DOI: 10.1016/j.ijthermalsci.2021.106973.
- [41] J.-F. Xie and B.-Y. Cao, "Natural convection of power-law fluids under wall vibrations: a lattice Boltzmann study," *Numerical Heat Transfer Part A Appl.*, vol. 72, no. 8, pp. 600–627, 2017. DOI: 10.1080/10407782. 2017.1394134.
- [42] S. Doley, V. K. Alagarsamy, A. J. Chamkha, J. Lawrence and A. Jacob, "Numerical study of heat transfer between hot moving material and ambient medium using various hybrid nanofluids under MHD radiative-convection, viscous dissipation effects, and time-fractional condition," *Numerical Heat Transfer Part B Fundament.*, vol. 84, no. 1, pp. 24–49, 2023. DOI: 10.1080/10407790.2023.2175745.
- [43] A. Divya, S. R. Sheri and A. K. Suram, "Finite element analysis of MHD naturally convective flow past an exponentially accelerated plate with viscous dissipation," *Numer. Heat Transfer Part B Fundament.*, vol. 85, no. 9, pp. 1115–1129, 2023. DOI: 10.1080/10407790.2023.2274454.
- [44] H. I. Andersson, K. H. Bech and B. S. Dandapat, "Magnetohydrodynamic flow of a power-law fluid over a stretching sheet," *Int. J. Non Linear Mechanics*, vol. 27, no. 6, pp. 929–936, 1992. DOI: 10.1016/0020-7462(92)90045-9.
- [45] G. R. Kefayati, "Simulation of ferrofluid heat dissipation effect on natural convection at an inclined cavity filled with kerosene/cobalt utilizing the lattice boltzmann method," *Numerical Heat Transfer Part A Appl.*, vol. 65, no. 6, pp. 509–530, 2014. DOI: 10.1080/10407782.2013.836022.
- [46] S. Acharya and S. K. Dash, "Natural convection in a cavity with undulated walls filled with water-based non-Newtonian power-law CuO-water nanofluid under the influence of the external magnetic field," Numer. Heat Transfer Part A Appl., vol. 76, no. 7, pp. 552–575, 2019. DOI: 10.1080/10407782.2019. 1644898.
- [47] H. C. Brinkman, "The viscosity of concentrated suspensions and solutions," J. Chem. Phys., vol. 20, no. 4, pp. 571–571, 1952. DOI: 10.1063/1.1700493.
- [48] V. M. Job and S. R. Gunakala, "Mixed convective ferrofluid flow through a corrugated channel with wall-mounted porous blocks under an alternating magnetic field," *Int. J. Mech. Sci.*, vol. 144, pp. 357–381, 2018. DOI: 10.1016/j.ijmecsci.2018.05.054.
- [49] D. Kushawaha, S. Yadav and D. K. Singh, "Magnetic field effect on double-diffusion with magnetic and non-magnetic nanofluids," *Int. J. Mech. Sci.*, vol. 191, pp. 106085, 2021. DOI: 10.1016/j.ijmecsci.2020. 106085
- [50] Z. A. S. Raizah, A. M. Aly and S. E. Ahmed, "Natural convection flow of a power-law non-Newtonian nanofluid in inclined open shallow cavities filled with porous media," *Int. J. Mech. Sci.*, vol. 140, pp. 376– 393, 2018. DOI: 10.1016/j.ijmecsci.2018.03.017.
- [51] S. V. Patankar, "Numerical heat transfer and fluid flow," Hemisp. Publish. Corporat. N. Y., 1980. DOI: 10. 1201/9781482234213.
- [52] T. Hayase, J. A. C. Humphrey and R. Greif, "A consistently formulated QUICK scheme for fast and stable convergence using finite-volume iterative calculation procedures," *J. Comput. Phys.*, vol. 98, no. 1, pp. 108–118, 1992. DOI: 10.1016/0021-9991(92)90177-Z.